



**HAL**  
open science

**Properties of Metal-Supported Oxide Honeycomb  
Monolayers:  $M_2O_3$  and  $MM'O_3$  on  $Me(111)$  ( $M, M'$   
 $= Ti, V, Cr, Fe; Me = Ag, Au, Pt$ )**

Jacek Goniakowski, C. Noguera

► **To cite this version:**

Jacek Goniakowski, C. Noguera. Properties of Metal-Supported Oxide Honeycomb Monolayers:  $M_2O_3$  and  $MM'O_3$  on  $Me(111)$  ( $M, M' = Ti, V, Cr, Fe; Me = Ag, Au, Pt$ ). *Journal of Physical Chemistry C*, 2020, 124 (15), pp.8186-8197. 10.1021/acs.jpcc.9b09337. hal-02875308

**HAL Id: hal-02875308**

**<https://hal.science/hal-02875308>**

Submitted on 19 Jun 2020

**HAL** is a multi-disciplinary open access archive for the deposit and dissemination of scientific research documents, whether they are published or not. The documents may come from teaching and research institutions in France or abroad, or from public or private research centers.

L'archive ouverte pluridisciplinaire **HAL**, est destinée au dépôt et à la diffusion de documents scientifiques de niveau recherche, publiés ou non, émanant des établissements d'enseignement et de recherche français ou étrangers, des laboratoires publics ou privés.

# Properties of Metal-Supported Oxide Honeycomb Monolayers: $M_2O_3$ and $MM'O_3$ on $Me(111)$ ( $M, M' = Ti, V, Cr, Fe; Me = Ag, Au, Pt$ )

J. Goniakowski\* and C. Noguera\*

*CNRS-Sorbonne Université, UMR 7588, INSP, F-75005 Paris, France*

E-mail: jacek.goniakowski@insp.jussieu.fr; claudine.noguera@insp.jussieu.fr

## Abstract

With the help of a DFT+U approach, we have analyzed the characteristics of a series of pure and mixed  $3d$  transition metal oxide honeycomb monolayers of  $M_2O_3$  and  $MM'O_3$  stoichiometries ( $M, M' = Ti, V, Cr$  and  $Fe$ ) deposited on a metal substrate ( $Me = Ag, Au, Pt$ ). We show that the substrate-induced structural polarization, interfacial electron transfer, and oxide-metal interaction strength display general trends which are governed by the offsets between the oxide band structure and the metal Fermi level. They are the strongest for the least electronegative cations ( $Ti$  and  $V$ ) deposited on supports with the largest work functions ( $Au, Pt$ ), where the depletion of purely  $3d$   $Ti$  and  $V$  states provokes an increase of the cation oxidation state. Mixing generally induces electron transfers from the least ( $Ti$  and  $V$ ) to the most ( $Cr$  and  $Fe$ ) electronegative cations. However, the systematic delocalization of the  $Ti_2O_3$   $d$  valence electrons to the metal substrates limits any significant mixing-induced electronic rearrangements to the  $V$ -based compounds only. We show that these electronic effects directly impact the energetics of cationic mixing and are responsible for a dramatic destabilization of the mixed  $TiFeO_3$  monolayers compared to the bulk ilmenite phase, while they stabilize ordered mixed  $VFeO_3$  films which have no bulk equivalent. Our findings give general guidelines

on how oxide electronic, magnetic and reactivity characteristics can be efficiently engineered by tuning the oxide stoichiometry and the metal substrate, of direct interest for modern technologies.

## 1 Introduction

Aside from van der Waals two-dimensional (2D) materials such as graphene, silicene, germanene, hexagonal boron nitride, or transition metal dichalcogenides, oxide monolayers (MLs) have recently attracted more and more interest due to their promising applications in the fields of catalysis and corrosion protection and to their relevance in the process of high-temperature oxide encapsulation of noble metal catalysts. Their properties are strongly affected by their reduced size and low dimensionality, which allows a large flexibility of their stoichiometry, atomic structure and electronic characteristics, often leading to complex compounds which have no bulk equivalents.<sup>1,2</sup> Moreover, the growing demand of methods for engineering the properties of such two-dimensional objects, fosters an efficient use of cation doping or mixing. Indeed, combining cations of different size, electronegativity and reducibility, may give a lever for modifying the oxide structural, electronic, and chemical reactivity characteristics.

Among the most frequently encountered oxide monolayer structures, the  $M_2O_3$  honeycomb (HC) one, which consists of a fully-coordinated network of twelve member rings with an equal number of oxygen and metal atoms, has been extensively studied experimentally and theoretically, whether freestanding,<sup>3</sup> or Pd(111)-,<sup>4,5</sup> Pt(111)-,<sup>6,7</sup> Au(111)-supported<sup>5,8-12</sup> as well as sandwiched between  $Al_2O_3$  films.<sup>13</sup> Aside its occurrence in sesquioxides monolayers, oxide honeycomb films have also been observed in  $Cu_3O_2/Au(111)$ ,<sup>14</sup> or used as a template for a synthesis of supported ternary  $Ba_xTi_2O_3/Au(111)$  compounds.<sup>15</sup>

Regarding cationic doping and mixing, we have recently shown that the low dimensionality of freestanding  $M_2O_3$  HC MLs and their peculiar, flat atomic structure determine their specific electronic characteristics (gap width, character of gap edges) and are responsible for cation redox reactions and mixing preferences which are different from those in the corresponding three-dimensional mixed oxides.<sup>3</sup> However, if these results provide guidelines for understanding properties of oxide films supported on very weakly interacting substrates, they are likely less relevant for the case of metal supports, which are the most widely used in practical realizations. Indeed, in another recent study, we have shown that the atomic structure of Au-supported  $M_2O_3$  HC MLs is characterized by a large structural rumpling and that the electronic characteristics of the freestanding films are severely altered by a charge exchange with the gold substrate, which in extreme cases may result in a change of cation oxidation state.<sup>9</sup>

In this context, the goal of the present theoretical work is twofold. On the one hand, beyond Au-supported  $M_2O_3$  MLs considered in our previous work,<sup>9</sup> we analyze the substrate-induced characteristics of pure  $M_2O_3$  and mixed  $MM'O_3$  oxide films ( $M, M' = Ti, V, Cr,$  and  $Fe$ ) deposited on three metallic substrates ( $Me = Ag, Au$  and  $Pt$ ) of higher and higher work functions. Relying on DFT+U results on freestanding and Me-supported MLs, we identify the mechanisms responsible for the most essential structural, electronic, and energetic characteristics of these supported films. On the other

hand, at variance with mixing at weakly or non-interacting interfaces,<sup>3</sup> we consider realistic situations by explicitly including the interaction with a metal substrate. To this goal we link the electronic and energetic characteristics of mixed  $MM'O_3/Me$  compounds to those of their pure  $M_2O_3/Me$  and  $M'O_3/Me$  parents and we assess the roles played by the character of the latter (Mott-Hubbard or charge transfer) and by the substrate work function.

The paper is organized as follows. After a section devoted to the computational method and set-up (Sec. 2), we report the results on Me-supported pure  $M_2O_3$  MLs (Sec. 3) and mixed  $MM'O_3$  MLs (Sec. 4). These results are then discussed in Sec. 5, before a conclusion.

## 2 Computational details

DFT calculations were performed with the Vienna Ab-initio Simulation Package (VASP)<sup>16,17</sup> using the Projector Augmented Wave (PAW) method<sup>18,19</sup> to represent the electron-core interaction and a 400 eV energy cut-off in the development of Kohn-Sham orbitals on a plane-wave basis set. We have checked that an increase of the cut-off to 500 eV does not bring any noticeable modifications to the reported results. For example, for  $VFeO_3$  and its parents  $Fe_2O_3$  and  $V_2O_3$ , regardless of the underlying metal, it changes the structural characteristics (film rumpling, anion-cation and cation-substrate bond lengths) by less than 0.01 Å, the electronic characteristics (anion, cation, and substrate charges) by less than 0.01 e/f.u. and the energetic ones (mixing energy) by less than 0.01 eV/f.u.

Dispersion-corrected (optB88-vdW)<sup>20-22</sup> exchange-correlation functional was employed, within the DFT+U approach proposed by Dudarev.<sup>23,24</sup> As in our previous studies,<sup>3,9,25,26</sup> we have used  $U$  values close to those reported in the literature:  $U = 1$  eV for  $Ti_2O_3$ ,  $U = 1.7$  eV for  $V_2O_3$ ,  $U = 3$  eV for  $Cr_2O_3$  and  $Fe_2O_3$ . Moreover we have performed complementary calculations using the HSE03 hybrid approach<sup>27,28</sup> to test the sensitivity of our results to the choice of the exchange-correlation

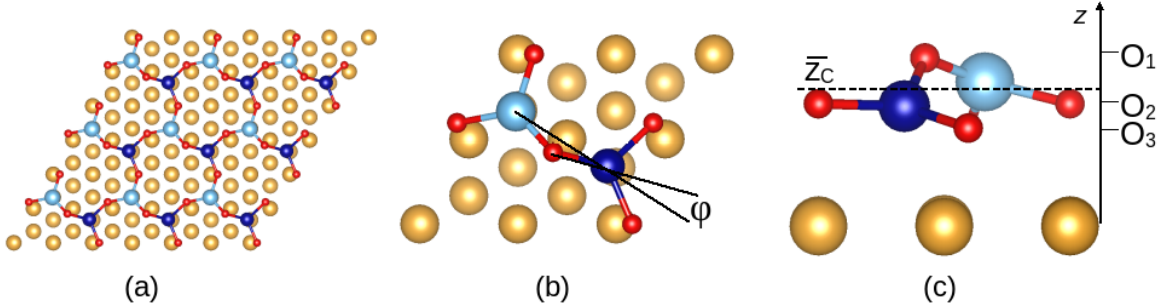


Figure 1: Atomic structures of Me-supported  $MM'O_3$  oxide ML: (a) top view; (b) enlarged top view showing the rotation  $\phi$  of the  $MO_3$  entities; c: enlarged profile view showing the rumpling of the layer, with the two cations and the three oxygen atoms at different elevations. The dashed line represents the average cation elevation  $\bar{z}_c$ . Cations, oxygen and substrate atoms are represented by blue (dark and light), red, and golden balls, respectively.

functional (Supporting Information (SI), Sec-  
 tions S2). As discussed in details in the case  
 of  $FeO_x/Pt$ ,<sup>29</sup> and pointed out in studies on  
 $CuO_2/Au$ <sup>14,30</sup> and  $MgO/Ag$ ,<sup>31</sup> despite the  
 known difficulties of the Hartree-Fock approach  
 to describe metals, the hybrid approximation  
 to the DFT gives a satisfactory description of  
 a metal/oxide interface and thus enables to  
 account for the oxide-metal band offset.

All calculations were spin-polarized and the  
 relative stability of simple non-magnetic (NM)  
 and magnetic solutions (with either parallel  
 (FM) or anti-parallel (AF) spin moments) was  
 systematically tested. Ionic charges were es-  
 timated with the partition scheme proposed  
 by Bader<sup>32,33</sup> and magnetic moments were ob-  
 tained by integration of the spin density within  
 the Bader's volumes. Atomic configurations  
 were plotted with VESTA.<sup>34</sup>

We have considered Me(111)-supported pure  
 $M_2O_3$  (the parents) and mixed  $MM'O_3$  mono-  
 layers ( $M, M' = Ti, V, Cr, \text{ and } Fe$ ;  $Me = Ag, Au$   
 and  $Pt$ ) in an honeycomb structure, Figure 1.  
 All of them were modelled in a  $(2 \times 2)$ -Me(111)  
 unit cell, with a single  $M_2O_3$  or  $MM'O_3$  formula  
 unit per cell, at the Me experimental bulk lat-  
 tice parameter (2.89 Å, 2.88 Å, and 2.765 Å  
 for Ag, Au and Pt, respectively), consistently  
 with experimental observations of pseudomor-  
 phic growth of ML  $Ti_2O_3$  on Au(111)<sup>10</sup> and  
 $V_2O_3$  on Pd(111).<sup>4</sup> The sampling of the Brill-  
 ouin zone was performed with the  $\Gamma$ -centered  
 $(14 \times 14 \times 1)$  Monkhorst-Pack mesh.<sup>35</sup> The metal

substrates were represented by slabs composed  
 of four (111) atomic layers. Increasing the  
 metal thickness up to 6 atomic layers yields neg-  
 ligible corrections on all quantities, consistently  
 with marginal (less than 0.05 eV) changes of the  
 metal work functions. The oxide film was de-  
 posited on one side of the metal slab. Be-  
 yond the symmetric film structures assumed  
 in Ref.,<sup>9</sup> all atomic coordinates of anions and  
 cations have been allowed to fully relax until  
 forces got lower than  $0.01 \text{ eV}\text{\AA}^{-1}$ . Atoms in  
 the metal substrates were relaxed only in the  
 direction normal to the surface. In the follow-  
 ing, the atomic structure of supported MLs will  
 be systematically quantified by the average film  
 rumpling  $R$  (defined as a difference of average  
 vertical positions of anions and cations  $\bar{z}_O - \bar{z}_C$ )  
 and by the average rotation of  $MO_3$  entities  
 $\phi = \angle(M' - M - O)$  projected on the surface  
 plane, Fig. 1.

Adhesion energies between the oxide mono-  
 layers and the metal substrates  $E_{adh}(Me)$  were  
 calculated from energy differences between the  
 constituted oxide/metal system  $E^{oxide/Me}$  and  
 its separated components (bare metal substrate  
 $E^{Me}$  and freestanding oxide ML at its equilib-  
 rium lattice parameter  $E^{oxide}$ ):

$$E_{adh}(Me) = E^{Me} + E^{oxide} - E^{oxide/Me} \quad (1)$$

With this definition, adhesion energies are pos-  
 itive if adhesion is favored.

Formation or mixing energies  $E_{mix}$  of both

freestanding and supported  $MM'O_3$  monolayers were calculated from energy differences between the mixed oxide  $E^{MM'O_3}$  and the average of the two corresponding parents  $(E^{M_2O_3} + E^{M'_2O_3})/2$ :

$$E_{mix}^{MM'O_3} = E^{MM'O_3} - \frac{E^{M_2O_3} + E^{M'_2O_3}}{2} \quad (2)$$

With this definition, mixing energies are negative if mixing is favored.

**Table 1: Main Characteristics of Freestanding and Me-supported (Me = Ag, Au and Pt)  $M_2O_3$  MLs (M = Ti, V, Cr, and Fe): Film Rumpling  $R$  (Å), In-Plane Rotation  $\phi$  ( $^\circ$ ), Bader Charges on Cations  $Q_M$  (e) and Oxygen Atoms  $Q_O$  (e), Total Charge of Metal Substrate  $Q_{Me}$  (e/ $M_2O_3$  f.u.), and Cation Magnetic Moments  $\mu_M$  ( $\mu_B$ ).**

	Ti <sub>2</sub> O <sub>3</sub>	V <sub>2</sub> O <sub>3</sub>	Cr <sub>2</sub> O <sub>3</sub>	Fe <sub>2</sub> O <sub>3</sub>
freestanding				
$Q_M$	1.78	1.69	1.62	1.64
$Q_O$	-1.19	-1.13	-1.08	-1.10
$\mu_M$	0.9	2.1	3.1	3.9
Ag-supported				
$R$	0.60	0.41	0.09	0.09
$\phi$	14	17	10	19
$Q_M$	1.92	1.72	1.55	1.44
$Q_O$	-1.06	-1.04	-1.08	-1.07
$\mu_M$	0.0	1.4/1.5	3.0	3.8
$Q_{Ag}$	-0.67	-0.33	+0.15	+0.33
Au-supported				
$R$	0.68	0.68	0.54	0.23
$\phi$	10	1	14	20
$Q_M$	2.00	1.83	1.65	1.53
$Q_O$	-1.02	-0.96	-0.96	-1.01
$\mu_M$	0.0	1.2	2.7	3.8
$Q_{Au}$	-0.94	-0.77	-0.42	-0.02
Pt-supported				
$R$	0.70	0.75	0.47	0.29
$\phi$	19	11	17	24
$Q_M$	2.00	1.87	1.65	1.50
$Q_O$	-1.01	-0.92	-0.96	-0.98
$\mu_M$	0.0	0.5	2.5	3.8
$Q_{Pt}$	-0.98	-0.98	-0.44	-0.06

### 3 Results on supported $M_2O_3$ monolayers

We first present the computational results for the  $M_2O_3$  HC monolayers (M = Ti, V, Cr, and Fe) supported on the three Me(111) substrates (Me = Ag, Au and Pt). Table 1 and Figure 2 report their main structural, electronic, and magnetic characteristics. The comprehensive set of results, is given in SI, Tabs. S1 and S2. HSE03 results for the  $M_2O_3$ /Au system (M = Ti, V, Cr, and Fe) are given in Tab. S7 and Fig. S1. In the following, the notation  $\Delta$  will refer to differences between quantities (positions, distances, charges, etc) in the supported and freestanding films

Fully relaxed freestanding oxide MLs systematically adopt a symmetric nearly planar geometry ( $R \sim 0$  and  $\phi \sim 0$ ). The only exception is the freestanding  $Cr_2O_3$  monolayer, for which we find a non-vanishing rumpling ( $R = 0.06$  Å). The interaction with the metal substrates and the in-plane compression associated to the lattice mismatch between the oxide films and metal surfaces ( $a_{M_2O_3} > a_{Me}$ , SI, Tab. S1) induce film distortion, which consists of in-plane rotations  $\phi$  of the  $MO_3$  entities and of rumpling  $R$ . We will show in the discussion that the positive sign of  $R$  (the average outward displacement of the oxygen atoms with respect to the cations), its decrease from Ti to Fe (for each substrate), and its increase from Ag to Pt (for each oxide) are principally driven by the behavior of the interface charge transfer  $Q_{Me}$ . Beyond the effect of film rumpling, the in-plane rotations  $\phi$  of the  $MO_3$  entities allow a further reduction of the in-plane oxide lattice parameters such that, despite substantial lattice mismatch, the cation-oxygen distances  $d_{M-O}$  remain in all cases close to the corresponding values in the freestanding MLs ( $|\Delta d_{M-O}/d_{M-O}| < 2\%$ , Tab. S1).

From an electronic point of view, the interaction of the oxide layers with the metallic substrates is characterized by an electron exchange between them, leading in most cases to a negative charging of the Me substrates (negative total substrate charge per  $M_2O_3$  unit,  $Q_{Me}$ ).

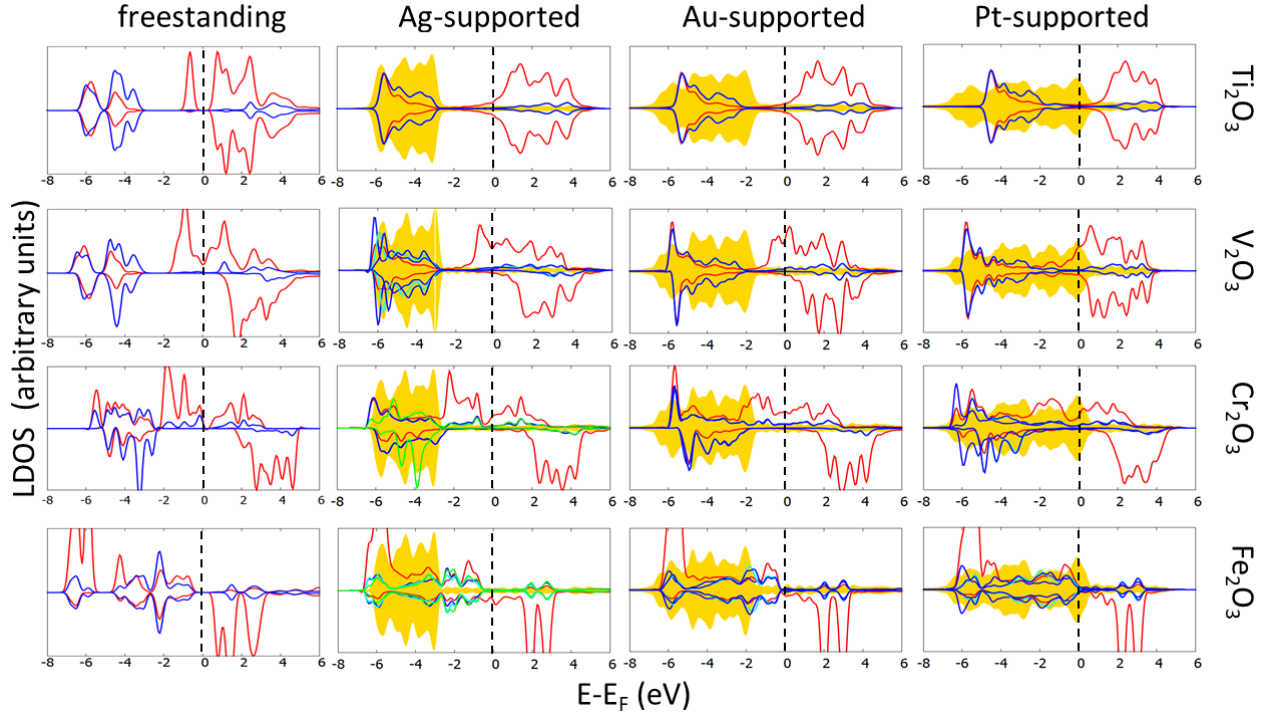


Figure 2: Local densities of states of freestanding and metal-supported  $M_2O_3$  HC MLs ( $M = \text{Ti}, \text{V}, \text{Cr},$  and  $\text{Fe}$ ) projected on cations (red), oxygen atoms (blue), and substrates (golden shading). A broadening of 0.2 eV has been systematically applied. The vertical dashed lines indicate the positions of the Fermi levels.

260 Small positive  $Q_{Me}$  are found only for  $\text{Cr}_2\text{O}_3$  284  
 261 and  $\text{Fe}_2\text{O}_3$  MLs deposited on the Ag substrate. 285  
 262 In the case of Ag and Au surfaces, where the 286  
 263 Fermi level is positioned relatively high in the 287  
 264 valence *sp* band, the substrate *d* states con- 288  
 265 tribute only little to the interfacial hybridiza- 289  
 266 tion and the electrons transferred from the ox- 290  
 267 ide film mainly populate the substrate *s* and 291  
 268 *p* orbitals. Conversely, since the Fermi level of 292  
 269 the Pt substrate falls in its 4*d* band, the Pt 293  
 270 *d* states hybridize strongly with those of the ox- 294  
 271 ide film and become populated by the interfa- 295  
 272 cial charge transfer. Finally the Ag electrons 296  
 273 transferred towards the  $\text{Cr}_2\text{O}_3$  and  $\text{Fe}_2\text{O}_3$  films 297  
 274 populate principally the cation *d* states at the 298  
 275 bottom of the oxide conduction band. As ex- 299  
 276 pected,  $|Q_{Me}|$  tends to decrease monotonically 300  
 277 from Ti to Fe (for each substrate), following 301  
 278 the increase of cation electronegativity, and in- 302  
 279 creases from Ag to Pt (for each oxide), following 303  
 280 the increase of the substrate surface work func- 304  
 281 tions (calculated values are 4.8 eV, 5.6 eV, and 305  
 282 6.1 eV for Ag, Au, and Pt, respectively). The 306  
 283 negative  $Q_{Me}$  result from a cooperative effect of 307

charge modifications on the oxide cations and oxygen atoms,  $Q_M$  increasing (except  $Q_{Fe}$ ) and  $|Q_O|$  decreasing when in contact with a support. The relative contributions of the oxygen atoms to  $|Q_{Me}|$  increase from Ti to Fe. Positive  $Q_{Me}$  are principally associated with a reduction of cation charges, the effect being particularly strong in the  $\text{Fe}_2\text{O}_3/\text{Ag}$  case.

Associated to this interfacial electron transfer, the oxide local densities of states (LDOS) are substantially modified. As seen in Figure 2, whatever the substrate, the modifications are particularly strong at the beginning of the series, in the Mott-Hubbard oxides  $\text{Ti}_2\text{O}_3$  and  $\text{V}_2\text{O}_3$ , where filled Ti and V 3*d* states close to the Fermi level get totally or partially depleted. At variance, due to the mixed oxygen-cation character of their states at the band gap edges, the band structures of  $\text{Cr}_2\text{O}_3$  and  $\text{Fe}_2\text{O}_3$  are much less impacted by the interaction with the metallic substrates.<sup>9</sup> For each oxide, the increase of the metal work function from Ag to Pt shifts the substrate Fermi level progressively downwards on the energy scale. As a conse-

308 quence, in  $\text{Ti}_2\text{O}_3$  which has a nearly pure Mott- 357  
 309 Hubbard character, the Fermi level  $E_F$  moves 358  
 310 from the bottom of the Ti-like conduction band 359  
 311 (CB) on Ag towards the oxide mid-gap on Pt. 360  
 312 The single valence  $d$  electron characteristic of 361  
 313 the freestanding  $\text{Ti}_2\text{O}_3$  ML is in all cases delo- 362  
 314 calized towards the underlying metal, which is 363  
 315 consistent with the substantial increase of  $Q_{\text{Ti}}$  364  
 316 and the systematic quenching of  $\mu_{\text{Ti}}$ , Tab. 1. 365  
 317 These major modifications of the  $\text{Ti}_2\text{O}_3$  elec- 366  
 318 tronic structure suggest that a change of oxi- 367  
 319 dation state takes place upon deposition. On 368  
 320 general grounds, at variance with the unques- 369  
 321 tionable 3+ cation valence in freestanding MLs, 370  
 322 changes of oxidation states in systems with de- 371  
 323 localized electrons cannot be assessed merely  
 324 from Bader charges. It is the concomitant mod-  
 325 ifications of the LDOS and magnetic moments  
 326  $\mu_{\text{Ti}}$  which can be tentatively rationalized by a  
 327 Ti 4+ oxidation state on the three substrates.

328 Similarly, in the case of the Mott-Hubbard ox- 374  
 329 ide  $\text{V}_2\text{O}_3$ , the progressive downward shift of the 375  
 330 Fermi level within the majority vanadium band 376  
 331 explains the increase of  $Q_V$  and the decrease of 377  
 332  $\mu_V$  along the Ag, Au, Pt series. These results 378  
 333 are consistent with a progressive increase of the 379  
 334 vanadium oxidation state in  $\text{V}_2\text{O}_3$  monolayer 380  
 335 supported on the three metal substrates. How- 381  
 336 ever, changes of V-O hybridization induced by 382  
 337 film distortions and the hybridization between 383  
 338 cation and substrate states (particularly strong 384  
 339 in case of Pt) impede a robust and fully reli- 385  
 340 able assignment of oxidation states in the three 386  
 341 cases. 387

342 Finally, in  $\text{Cr}_2\text{O}_3$  and  $\text{Fe}_2\text{O}_3$  the shape of the 388  
 343 oxide LDOS in the vicinity of the Fermi level 389  
 344 is very similar on the three substrates. Consis- 390  
 345 tently, changes of  $Q_M$  and  $\mu_M$  with respect to 391  
 346 the freestanding references are similarly small 392  
 347 on the three substrates and suggest that the 393  
 348 cation 3+ oxidation states are essentially not 394  
 349 altered. 395

350 To summarize, the interaction with the metal 396  
 351 substrates induces structural distortions of the 397  
 352 oxide MLs and an electron transfer from the 398  
 353 oxides towards the metal, which both increase 399  
 354 from Ag to Pt and decrease from Ti to Fe. 400  
 355 Only when  $\text{Cr}_2\text{O}_3$  and  $\text{Fe}_2\text{O}_3$  are deposited on 401  
 356 Ag a small amount of electrons is transferred 402

from the substrate towards the oxide film. The  
 substrate-induced change of oxide electronic  
 and magnetic characteristics is particularly pro-  
 nounced in  $\text{Ti}_2\text{O}_3$  and  $\text{V}_2\text{O}_3$ , where it can be as-  
 sociated to an increase of cation oxidation state.  
 If the single Ti valence electron tends to be sys-  
 tematically transferred to the metal substrate,  
 the cation charge of supported  $\text{V}_2\text{O}_3$  increases  
 progressively from Ag to Pt. Conversely, the  
 much weaker electronic modifications found for  
 $\text{Cr}_2\text{O}_3$  and  $\text{Fe}_2\text{O}_3$  suggest the preservation of  
 the cation 3+ oxidation state characteristic of  
 the freestanding MLs. These conclusions are  
 well supported by the HSE03 results (SI, Tab.  
 S7).

## 4 Results on supported $\text{MM}'\text{O}_3$ monolayers

DFT+U results for the main structural, elec-  
 tronic and magnetic characteristics of free-  
 standing and Me-supported mixed  $\text{MM}'\text{O}_3$  HC  
 MLs (M, M' = Ti, V, Cr, and Fe; Me = Ag,  
 Au, Pt) are given in Table 2 and Figures 3 and  
 4. The complete set of results can be found in  
 SI, Tabs. S4 and S5, in which the symbols  $\delta$   
 denote the mixing-induced differences between  
 quantities (positions, distances, charges, etc) in  
 the supported mixed oxides and their parents.  
 HSE03 results for mixed MLs on the Au sub-  
 strate are reported in SI, Tab. S8 and Fig. S2.

From a structural point of view, the metal-  
 supported mixed oxide films are qualitatively  
 similar to their supported parents. They  
 systematically display a substantial (positive)  
 rumpling and in-plane rotations of  $\text{MO}_3$  entities  
 which enable an accommodation of the inter-  
 face lattice mismatch without strong modifica-  
 tions of the cation-oxygen distances  $d_{M-O}$  and  
 $d_{M'-O}$  ( $|\Delta d_{M-O}/d_{M-O}| < 4\%$ , Tab. S4). Con-  
 trary to the parent systems, in the mixed films  
 the two cations are systematically not coplanar.  
 Cationic mixing produces a quite substantial  
 rumpling enhancement ( $\delta R \sim 0.15 - 0.25 \text{ \AA}$ ) in  
 $\text{VCrO}_3/\text{Ag}$ ,  $\text{VFeO}_3/\text{Pt}$ , and  $\text{CrFeO}_3/\text{Pt}$ , but in  
 $\text{TiFeO}_3/\text{Ag}$ ,  $\text{TiCrO}_3/\text{Au}$ , and  $\text{VCrO}_3/\text{Au}$ ,  $R$  is  
 reduced ( $\delta R \sim -0.10 \text{ \AA}$ ), Tab. S4. We will show  
 in the discussion that the positive sign and the

**Table 2: Main Characteristics of Metal (Ag, Au, and Pt)-Supported Mixed MM'O<sub>3</sub> HC Monolayers (M, M' = Ti, V, Cr, and Fe): Film Rumpling  $R$  (Å), In-Plane Rotation  $\phi$  (°), Bader Charges on Cations  $Q_M, Q'_M$  (e) and Oxygen Atoms  $Q_O$  (e), Metal Substrate Charge  $Q_{Me}$  (e/MM'O<sub>3</sub> f.u.), and Cation Magnetic Moments  $\mu_M, \mu_{M'}$  ( $\mu_B$ ).**

	TiVO <sub>3</sub>	TiCrO <sub>3</sub>	TiFeO <sub>3</sub>	VCrO <sub>3</sub>	VFeO <sub>3</sub>	CrFeO <sub>3</sub>
freestanding						
$Q_M, Q_{M'}$	1.75,1.69	1.80,1.55	2.09, 1.33	1.84, 1.47	1.87, 1.35	1.67, 1.60
$Q_O$	-1.15	-1.12	-1.14	-1.10	-1.08	-1.09
$\mu_M, \mu_{M'}$	1.0, 2.0	0.9, 3.2	0.1, 3.6	1.4, 3.6	1.3, 3.6	2.7, 4.0
Ag-supported						
$R$	0.50	0.41	0.23	0.47	0.35	0.06
$\phi$	15	19	19	18	19	18
$Q_M, Q_{M'}$	1.91,1.73	1.93,1.58	1.95,1.38	1.81,1.46	1.82,1.35	1.60,1.37
$Q_O$	-1.05	-1.06	-1.09	-1.00	-1.01	-1.08
$\mu_M, \mu_{M'}$	0.2,1.4	0.2,2.9	0.1,3.7	0.7,3.4	0.,3.7	2.6,3.7
$Q_{Ag}$	-0.47	-0.33	-0.05	-0.27	-0.15	0.27
Au-supported						
$R$	0.69	0.52	0.45	0.49	0.50	0.35
$\phi$	5	16	19	16	16	20
$Q_M, Q_{M'}$	1.99,1.86	2.01,1.67	2.01,1.54	1.93,1.51	1.94,1.42	1.69,1.51
$Q_O$	-0.99	-1.02	-1.03	-0.98	-0.96	-1.00
$\mu_M, \mu_{M'}$	0.1,0.9	0.1,2.8	0.1,3.9	0.5,3.4	0.0,3.7	2.2,3.9
$Q_{Au}$	-0.88	-0.60	-0.45	-0.50	-0.48	-0.21
Pt-supported						
$R$	0.74	0.61	0.52	0.68	0.67	0.62
$\phi$	15	20	24	18	18	19
$Q_M, Q_{M'}$	1.97,1.91	1.98,1.69	2.00,1.55	1.94,1.62	1.96,1.49	1.75,1.47
$Q_O$	-0.95	-0.97	-1.00	-0.92	-0.91	-0.89
$\mu_M, \mu_{M'}$	0.0,0.0	0.1,2.3	0.1,4.0	0.3,2.8	0.1,3.9	1.3,3.9
$Q_{Pt}$	-1.04	-0.76	-0.54	-0.80	-0.70	-0.55

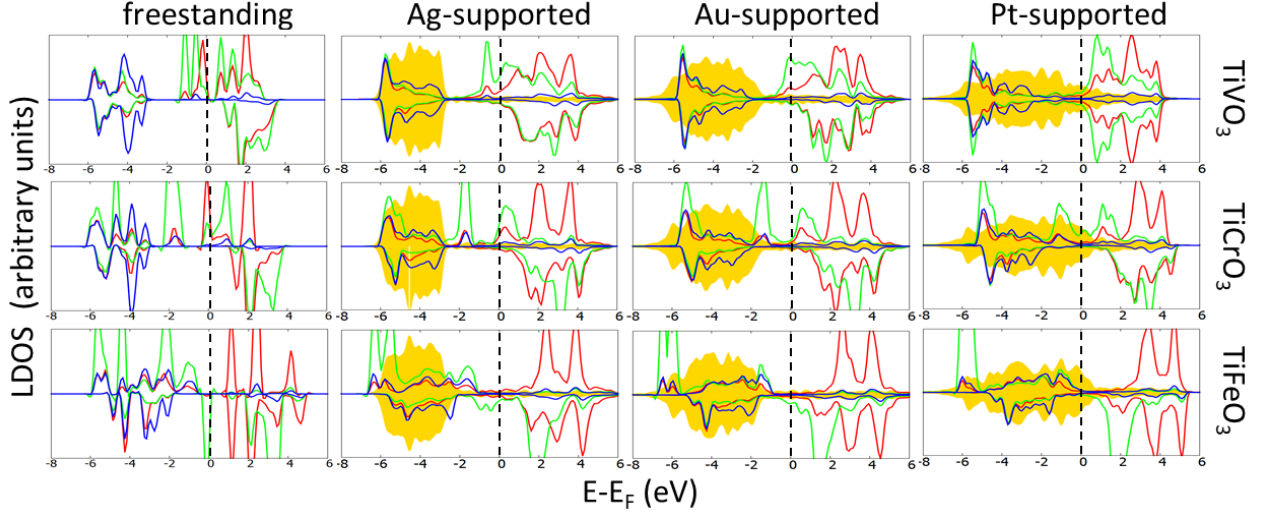


Figure 3: Local densities of states in freestanding and Me-supported mixed  $\text{TiM}'\text{O}_3$  honeycomb monolayers ( $M' = \text{V, Cr, Fe}$ ) projected on Ti (red),  $M'$  (green), O atoms (blue), and substrate atoms (gold shading). A broadening of 0.2 eV has been systematically applied. Vertical dashed lines indicate the position of the Fermi level.

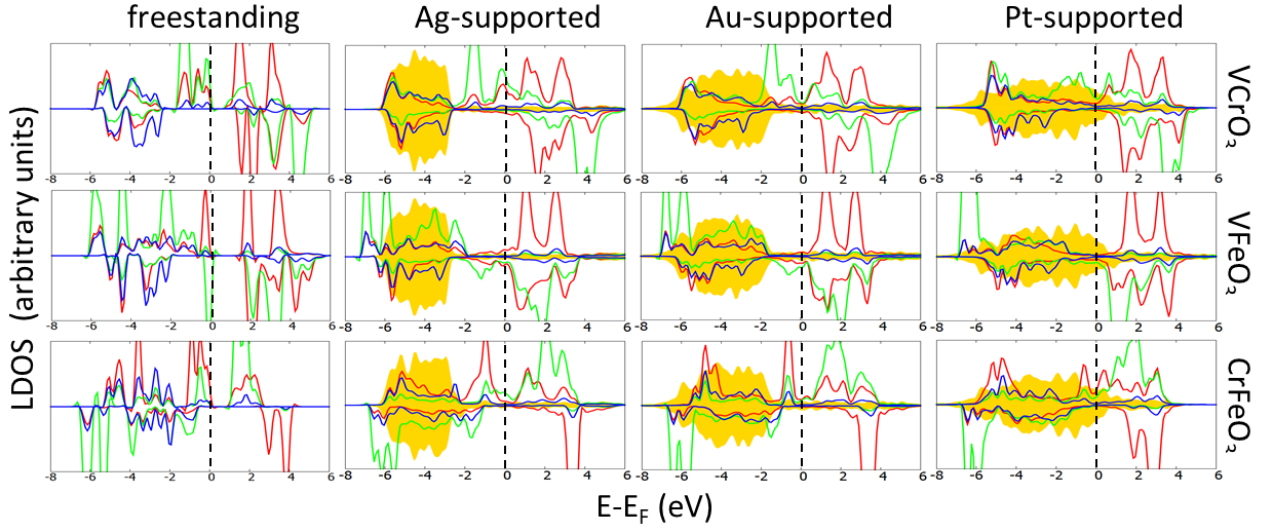


Figure 4: Local densities of states in freestanding and Me-supported mixed  $\text{MM}'\text{O}_3$  honeycomb monolayers ( $M = \text{V, Cr}$ ;  $M' = \text{Cr, Fe}$ ) projected on M (red),  $M'$  (green), O atoms (blue), and substrate atoms (gold shading). A broadening of 0.2 eV has been systematically applied. Vertical dashed lines indicate the position of the Fermi level.

403 amplitude of  $R$  are mainly driven by the behav- 452  
404 ior of the interface charge transfer  $Q_{Me}$ . 453

405 Similarly to most supported  $M_2O_3$  parents, 454  
406 the interaction of the mixed films with the 455  
407 metallic substrates gives rise to a systematic 456  
408 electron transfer from the oxide towards the 457  
409 substrate ( $Q_{Me} < 0$ ), but in  $CrFeO_3/Ag$  where 458  
410 electrons are transferred towards the oxide film 459  
411 ( $Q_{Me} > 0$ ). Both cations and anions contribute 460  
412 to the interface charge transfer and the per- 461  
413 centage weight of oxygen contributions progres- 462  
414 sively increases along the oxide series. At each 463  
415 of the three substrates  $|Q_{Me}|$  decreases follow- 464  
416 ing the increasing average electronegativity of 465  
417 the two cations ( $TiVO_3 < TiCrO_3 < VCrO_3 <$  466  
418  $TiFeO_3 < VFeO_3 < CrFeO_3$ ). For each oxide 467  
419 it increases from Ag to Pt in line with the in- 468  
420 creasing substrate work functions. As a conse- 469  
421 quence, cation charges  $Q_{M,M'}$  increase and oxy- 470  
422 gen charges  $|Q_O|$  decrease when moving from 471  
423 Ag to Pt. Only  $Q_{Ti}$  values change particularly 472  
424 little from one substrate to another in all sup- 473  
425 ported  $TiM'O_3$  compounds. 474

426 In our previous study on freestanding films,<sup>3</sup> 475  
427 we have pointed out that the electronic mod- 476  
428 ifications in  $TiVO_3$ ,  $TiCrO_3$ , and  $CrFeO_3$  due 477  
429 to mixing are small since their cationic charges 478  
430 and magnetic moments are close to those in the 479  
431 corresponding freestanding parents, and their 480  
432 LDOS differ little from a superposition of the 481  
433 parent LDOS. Conversely, in  $TiFeO_3$ ,  $VCrO_3$ , 482  
434 and  $VFeO_3$ , a well pronounced increase of  $Q_M$  483  
435 and a decrease of  $Q_{M'}$ , correlated with strong 484  
436 modifications of cation magnetic moments and 485  
437 LDOS peak positions with respect to the Fermi 486  
438 level, have been rationalized in terms of mixing- 487  
439 induced redox reactions, leading to  $Ti^{4+}Fe^{2+}$ , 488  
440  $V^{4+}Cr^{2+}$ , and  $V^{4+}Fe^{2+}$  oxidation states, respec- 489  
441 tively. 490

442 The presence of the metal substrates visibly 491  
443 alters this picture. In contrast to the freestand- 492  
444 ing case, supported  $TiFeO_3$  displays only neg- 493  
445 ligible mixing-induced electronic modifications, 494  
446 regardless of the metal support (Tab. 2 and 495  
447 1 and Fig. 2, 3 and 4). Moreover, while, 496  
448 similarly to the freestanding films, the mixing-  
449 induced changes in  $VFeO_3$  and  $VCrO_3$  are the  
450 most pronounced, the underlying electron re-  
451 distributions do not follow the same pattern

on the three substrates. Indeed, on Ag and Au substrates, the changes mostly consist of an electron exchange between the two cations ( $\delta Q_V \approx -\delta Q_{Cr,Fe}$ , Tab. S5), and are associated with opposite shifts of the V and Cr/Fe states in the vicinity of the Fermi level (see Fig. 4). In these mixed oxides also the modifications of oxygen charges  $\delta Q_O$  provide a non-negligible contribution to  $\delta Q_{Me}$ . Conversely, on the Pt substrate the largest modifications concern only vanadium cations, which points toward an increase of the vanadium oxidation state stabilized by an electron transfer towards the metal substrate  $\delta Q_{Pt}$ . These different behaviors illustrate the competition between electron transfer between the two cations and from a cation to the substrate, governed by the availability and nature of the oxide electronic states in the vicinity of the Fermi level. At variance with the above, the electronic characteristics of supported  $TiVO_3$  and  $TiCrO_3$  films remain relatively close to those of their supported parents, as was the case for their freestanding counterparts. Finally,  $CrFeO_3$  displays an intermediate behavior. On Ag and Au, mixing-induced modifications are relatively weak, but on Pt,  $\mu_{Cr}$  is visibly reduced. These changes, together with the complex DOS modifications (see Fig. 4) do not allow a clear assignment of a change of oxidation state.

To summarize, the structural ( $R$ ) and electronic ( $Q_{Me}$ ) characteristics of the supported pure and mixed oxide films follow qualitatively similar trends. The electronic characteristics of  $TiVO_3$ ,  $TiCrO_3$ , and  $TiFeO_3$  correspond closely to a superposition of those of their parents. Conversely, in Ag- and Au- supported  $VCrO_3$  and  $VFeO_3$  mixing induces an electron transfer from V to either Cr or Fe. It is much stronger in  $VFeO_3$  and can be tentatively interpreted as a redox reaction. Interestingly, on the Pt substrate, the electrons are rather transferred from V to the metal substrate. These conclusions are well supported by HSE03 results given in SI, Tab. S8 and Fig. S2.

## 5 Discussion

498 In this section, we first discuss the mechanisms  
 499 which govern the electronic and structural char-  
 500 acteristics of metal-supported HC oxides upon  
 501 interaction with the substrate (Section 5.1) and  
 502 upon cation mixing (Section 5.2). Then we ana-  
 503 lyze the evolution of the oxide adhesion (Section  
 504 5.3) and mixing (Section 5.4) energies.

### 5.1 Electron redistribution at the oxide/metal interface

507 In our recent study on the Au-supported pure  
 508  $M_2O_3$  monolayers,<sup>9</sup> we have shown that the  
 509 interfacial charge transfer  $Q_{Au}$  and its conse-  
 510 quences on the electronic characteristics of the  
 511 deposited oxide films may be reliably inferred  
 512 from the offset between the point of zero charge  
 513 of the freestanding oxide films  $E_{ZCP}$  (approx-  
 514 imated by the energy at mid-gap position) with  
 515 respect to the Fermi level of the bare Au sur-  
 516 face  $E_F(Au)$  and from the character of the oxide  
 517 gap edges. We have shown that the decrease of  
 518  $|Q_{Au}|$  along the series of transition metal ox-  
 519 ides is due to the progressive lowering of the  
 520 point of zero charge, mainly due to the increase  
 521 of the cation electronegativity. This argument  
 522 is generalized in Figure 5 to the parents and  
 523 mixed oxide MLs deposited on the three sub-  
 524 strates. Corresponding results from hybrid calcu-  
 525 lations on Au-supported  $M_2O_3$  and  $MM'O_3$   
 526 compounds are reported in SI, Fig. S3.

527 In agreement with the results of Ref.,<sup>9</sup> we  
 528 find that, for each substrate and regardless of  
 529 the pure or mixed oxide character, the interface  
 530 charge transfer correlates well with  $E_F(Me) -$   
 531  $E_{ZCP}$ . As a consequence,  $Q_{Me}$  is systemati-  
 532 cally the most negative for  $M_2O_3$  oxides with  
 533 the least electronegative cations (Ti, V), and  
 534 for mixed oxides with the smallest average  
 535 cation electronegativity ( $TiVO_3$ ,  $TiCrO_3$ , and  
 536  $VCrO_3$ ). Conversely, small positive  $Q_{Me}$  val-  
 537 ues are found for  $Cr_2O_3$ ,  $Fe_2O_3$  and  $CrFeO_3$ .  
 538 Moreover, for each oxide, the substrate charge  
 539 becomes more negative along the Ag, Au, and  
 540 Pt series, following the increase of the work  
 541 functions of the metal surfaces (4.8 eV, 5.6 eV,  
 542 and 6.1 eV, respectively). Such quasi-linear be-

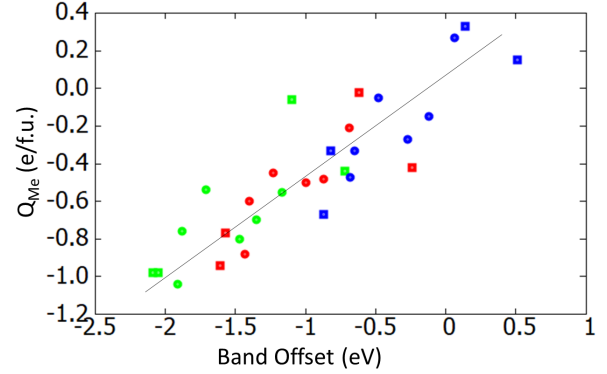


Figure 5: Interface charge transfer  $Q_{Me}$  ( $e/M_2O_3$  or  $MM'O_3$  f.u.) as a function of the offset  $E_F(Me) - E_{ZCP}$  (eV) between the Fermi level of the bare metal surface and the point of zero charge of the freestanding pure (squares) and mixed (circles) oxide monolayers. Results for Ag, Au, and Pt substrates are plotted with blue, red, and green symbols, respectively. Line is drawn to guide the eye.

543 haviour of the interface charge transfer as a  
 544 function of the band offset agrees well with the  
 545 predictions of the Metal-Induced Gap States  
 546 (MIGS) model at metal/semiconductor inter-  
 547 faces.<sup>36,37</sup>

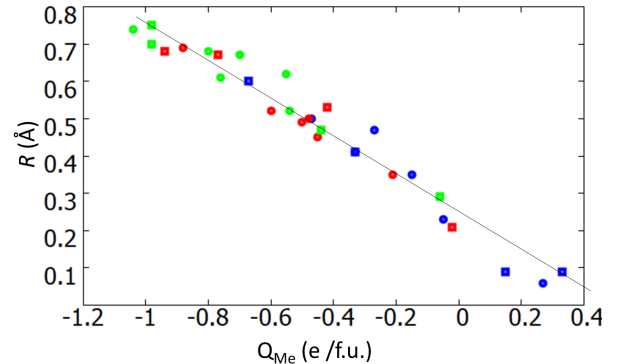


Figure 6: Average rumpling  $R$  ( $\text{\AA}$ ) in supported pure  $M_2O_3$  (squares) and mixed  $MM'O_3$  (circles) MLs as a function of the electron transfer  $Q_{Me}$  ( $e/M_2O_3$  or  $MM'O_3$  f.u.) Results for  $Me = Ag, Au,$  and  $Pt$  substrates are represented in blue, red, and green, respectively. Line is drawn to guide the eye.

548 Metal-supported oxide monolayers undergo  
 549 structural distortions in response to the electro-  
 550 static dipole produced by the interface charge

transfer  $Q_{Me}$ .<sup>38,39</sup> Based on a simple electro-  
static argument, a negatively charged substrate  
( $Q_{Me} < 0$ ) repels the anions and thus tends to  
produce a positive rumpling ( $R > 0$ ) whereas  
a negative rumpling is expected for a positive  
charging of the substrate. The induced struc-  
tural dipole of the oxide film which results from  
such electrostatic coupling between charge and  
structure has been baptized induced polarity.<sup>38</sup>  
In agreement with this argument, we find that,  
for each substrate and regardless of the pure  
or mixed oxide character, the film rumpling  $R$   
correlates very well with the interface charge  
transfer  $Q_{Me}$ . As a consequence,  $R$  is system-  
atically the largest for oxides which transfer the  
largest number of electrons to the metal sub-  
strates ( $\text{Ti}_2\text{O}_3$ ,  $\text{V}_2\text{O}_3$ ,  $\text{TiVO}_3$ ). Conversely, the  
smallest film rumpling is systematically found  
for  $\text{Fe}_2\text{O}_3$ ,  $\text{Cr}_2\text{O}_3$  and  $\text{CrFeO}_3$ . Moreover, rum-  
pling of each oxide film increases when moving  
from Ag to Pt, following the corresponding in-  
crease of the electron transfer. We stress that  
such an excellent unique  $R \propto Q_{Me}$  relationship  
obtained for a variety of oxide films on various  
metal substrates is likely due to a negligible ef-  
fect of lattice mismatch on  $R$ , the latter being  
rather accommodated by in-plane rotations.

At this point it is worth noting that the mono-  
tonic decrease of  $R$  is associated with more com-  
plex film structure. Indeed, while large rum-  
pling values (large negative  $Q_{Me}$ ) are systemat-  
ically associated to an outward relaxation of the  
three oxygen atoms (per f.u.) with respect to  
the cation planes, in  $\text{Fe}_2\text{O}_3$ ,  $\text{Cr}_2\text{O}_3$ , and  $\text{CrFeO}_3$   
on Ag (the smallest  $R$  and positive  $Q_{Me}$  values),  
although  $R$  remains positive, two oxygen atoms  
are located below the average cation positions  
(SI Tables S1 and S4). In case of oxides which  
display the smallest negative  $Q_{Me}$  ( $\text{Fe}_2\text{O}_3$  on Au  
and Pt,  $\text{TiFeO}_3/\text{Ag}$ ), only one oxygen atom is  
located below the cation plane or two oxygen  
atoms are nearly coplanar with the cations.

To summarize, we have shown that the elec-  
tron transfer between the oxides and the metal  
substrate is mainly driven by the offset between  
the oxide band structure (point of zero charge)  
and the substrate Fermi level. As a conse-  
quence, the strongest electron redistributions  
(large negative  $Q_{Me}$ ) are found in oxides with

the least electronegative cations (Ti and V) de-  
posited on metal substrates with the largest  
work functions (Au, Pt). Moreover, we find  
that the interface electron transfer determines  
the behavior of the substrate-induced film po-  
larization (rumpling) and is responsible for  
its progressive decrease from the least ( $\text{Ti}_2\text{O}_3$ ,  
 $\text{V}_2\text{O}_3$ ,  $\text{TiVO}_3$ ) to the most ( $\text{Fe}_2\text{O}_3$ ,  $\text{Cr}_2\text{O}_3$ , and  
 $\text{CrFeO}_3$ ) electronegative compounds.

## 5.2 Electron redistribution upon cationic mixing

While the previous section dealt with the mod-  
ifications of the oxide ML atomic and elec-  
tronic structure due to their interaction with  
the metallic substrates, here we focus on those  
which take place upon cationic mixing.

In the past we have successfully rational-  
ized the electronic characteristics of mixed bulk  
 $\text{MM}'\text{O}_3$  materials,<sup>25</sup> freestanding  $\text{MM}'\text{O}_3$  hon-  
eycomb monolayers,<sup>3</sup> and  $\text{M}_2\text{O}_3/\text{M}'_2\text{O}_3$  inter-  
faces,<sup>26</sup> from the band offsets between the cor-  
responding parent  $\text{M}_2\text{O}_3$  and  $\text{M}'_2\text{O}_3$  materials. In  
the present case, a similar analysis can be based  
on a comparison between the LDOS of the four  
metal-supported parents on an energy scale de-  
fined by their common vacuum level, Fig. 7.  
As a reference, the corresponding results for  
the freestanding HC MLs are recalled. Corre-  
sponding HSE03 results on  $\text{M}_2\text{O}_3/\text{Au}$  HCs are  
reported in SI, Figure S4.

The band offset between any couple of par-  
ents is quantified by the difference of positions  
of their Fermi levels  $\Delta E_F = E_F(\text{M}_2\text{O}_3/\text{Me}) -$   
 $E_F(\text{M}'_2\text{O}_3/\text{Me})$ , such that positive and neg-  
ative values of  $\Delta E_F$  indicate an initial bias  
for  $\text{M}_2\text{O}_3/\text{Me} \rightarrow \text{M}'_2\text{O}_3/\text{Me}$  and  $\text{M}'_2\text{O}_3/\text{Me} \rightarrow$   
 $\text{M}_2\text{O}_3/\text{Me}$  electron transfers, respectively. Be-  
yond the relative positions of the Fermi levels  
 $\Delta E_F$ , the actual possibility of the charge trans-  
fer as well as the precise origin and destination  
of the transferred electrons also depend on the  
character of the occupied and empty states in  
the vicinity of the Fermi level.

While the ordering of Fermi level positions in  
the freestanding parents was qualitatively de-  
termined by the cation electronegativity differ-  
ence, in the supported ones, it is rather due

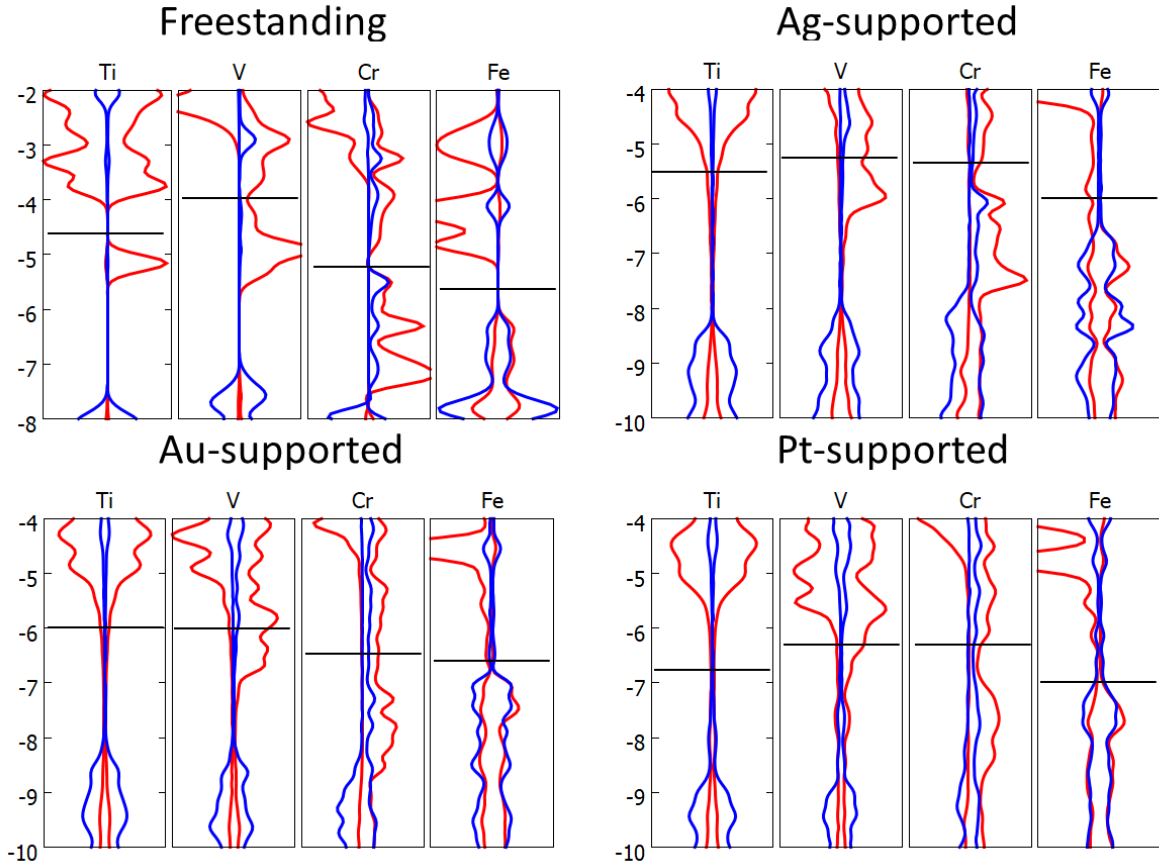


Figure 7: LDOS of the freestanding and Me-supported pure  $M_2O_3$  monolayers ( $M = \text{Ti}, \text{V}, \text{Cr}, \text{Fe}$ ) in the vicinity of their Fermi level (marked by the horizontal black lines), projected on cations (red), and oxygen atoms (blue), on an energy scale obtained by alignment of the common vacuum level. A broadening of 0.2 eV has been systematically applied.

647 to the change in metal work function induced 687  
 648 by the deposition of an oxide film  $\Delta W$ . Cal- 688  
 649 culated  $\Delta W$  for the four parents are given in 689  
 650 Table 3. We note that, since at each substrate 690  
 651 the largest values are systematically found for 691  
 652  $\text{Fe}_2\text{O}_3$  and the smallest ones for  $\text{V}_2\text{O}_3$ , the re- 692  
 653 sulting ordering of Fermi level positions is not 693  
 654 strongly modified compared to that found in 694  
 655 the freestanding films. 695

**Table 3: Change of the Metal Work Function  $\Delta W$  (eV) upon Deposition of Pure HC Monolayers.**

	$\text{Ti}_2\text{O}_3$	$\text{V}_2\text{O}_3$	$\text{Cr}_2\text{O}_3$	$\text{Fe}_2\text{O}_3$
$\Delta W_{Ag}$	0.62	0.38	0.45	1.15
$\Delta W_{Au}$	0.36	0.44	0.80	0.95
$\Delta W_{Pt}$	0.75	0.15	0.17	0.89

656 We recall that  $\Delta W$  is determined by the 705  
 657 dipole moment of the oxide/metal inter- 706  
 658 face, which consists of three main contribu- 707  
 659 tions.<sup>38,40,41</sup> The first one comes from the re- 708  
 660 duction of the substrate surface dipole caused 709  
 661 by the compression of the spilled-out metal elec- 710  
 662 trons by the deposited oxide monolayer. The 711  
 663 second one is induced by the electron exchange 712  
 664  $Q_{Me}$  between the oxide film and the metallic 713  
 665 substrate. The third one is due to the struc- 714  
 666 tural film polarization (rumpling)  $R$ . While the 715  
 667 first effect produces a negative contribution to 716  
 668  $\Delta W$ , and while a positive film rumpling ( $R >$  717  
 669 0) tends to increase  $R$ , the contribution due 718  
 670 to electron exchange at the interface either de- 719  
 671 creases (negative  $Q_{Me}$ ) or increases (positive 720  
 672  $Q_{Me}$ ) the substrate work function. 721

673 In the present case, the systematically pos- 722  
 674 itive signs of  $\Delta W$ , Tab. 3, suggest that the 723  
 675 rumpling contribution is dominant, aided by 724  
 676 the charge transfer term in the few cases where 725  
 677  $Q_{Me}$  is positive. However, since the largest  $\Delta W$  726  
 678 values ( $\text{Fe}_2\text{O}_3$  on the three substrates) system- 727  
 679 atically correspond to the smallest rumplings 728  
 680  $R$ , the behavior of  $\Delta W$  along the series of ox- 729  
 681 ides is clearly not rumpling-driven. The largest 730  
 682  $\Delta W$ , responsible for the most pronounced band 731  
 683 offsets between parent materials, rather corre- 732  
 684 spond to positive or small negative values of 733  
 685 the charge transfer contribution. It should be 734  
 686 noted that in-plane rotation  $\phi$  may also play 735

a role since the largest values in Tab. 3 also correspond to the largest rotations.

Solely from the signs of  $\Delta E_F$ , Fig. 7, one deduces that an electron transfer may systematically occur from  $\text{Ti}_2\text{O}_3/\text{Me}$  or  $\text{V}_2\text{O}_3/\text{Me}$  toward  $\text{Fe}_2\text{O}_3/\text{Me}$  ( $\text{Me} = \text{Ag}, \text{Au}$  and  $\text{Pt}$ ) or  $\text{Cr}_2\text{O}_3/\text{Au}$ , and from  $\text{Cr}_2\text{O}_3/\text{Me}$  toward  $\text{Fe}_2\text{O}_3/\text{Me}$  ( $\text{Me} = \text{Ag}$  and  $\text{Pt}$ ). No electron exchange is expected between  $\text{Ti}_2\text{O}_3/\text{Me}$  and  $\text{V}_2\text{O}_3/\text{Me}$  except on  $\text{Pt}$ , where an electron transfer from  $\text{V}_2\text{O}_3$  to  $\text{Ti}_2\text{O}_3$  could be anticipated. If additionally the character and the density of states at the Fermi level are taken into account, it becomes clear that supported  $\text{Ti}_2\text{O}_3$  is unlikely to provide electrons to  $\text{Cr}$  or  $\text{Fe}$  upon mixing because it has no available occupied cationic  $d$  states. Also the electron transfer from  $\text{V}_2\text{O}_3$  to  $\text{Ti}_2\text{O}_3$  on  $\text{Pt}$  is impeded by the absence of empty  $\text{Ti}$   $d$  states in the energy range between the two Fermi levels. As a consequence, no significant mixing-induced charge redistribution is expected in all  $\text{Ti}$ -containing compounds. Conversely, since a significant number of occupied cationic states just below the Fermi level exist in  $\text{V}_2\text{O}_3/\text{Me}$ , an electron transfer from  $\text{V}_2\text{O}_3/\text{Me}$  towards  $\text{Fe}_2\text{O}_3/\text{Me}$  is systematically to be expected, as well as a transfer from  $\text{V}_2\text{O}_3/\text{Au}$  towards  $\text{Cr}_2\text{O}_3/\text{Au}$ . We note that the absence of empty  $\text{Fe}_2\text{O}_3$  states in the direct vicinity of the Fermi level may produce an electron transfer toward the metal substrate rather than toward the  $\text{Fe}$  cations. Finally, the limited number of occupied (empty) states at  $E_F$  in  $\text{Cr}_2\text{O}_3/\text{Me}$  ( $\text{Fe}_2\text{O}_3/\text{Me}$ ) may hinder electron redistribution in  $\text{CrFeO}_3/\text{Me}$ . These predictions correlate very well with the results of the full calculations, Sec. 4.

To summarize, the relative positions of the Fermi levels in the supported parents provide a good guide for understanding the electronic redistributions in the mixed compounds. While the ordering of Fermi levels in the series of parent oxides is not strongly modified by the metal substrate, we have pointed out that the character of the oxide states in the vicinity of the Fermi level is. For the series of supported  $\text{MM}'\text{O}_3$  HC MLs, the offsets between the parent band structures and the absence of  $\text{Ti}$   $d$  states in the the Fermi level vicinity

in supported  $\text{Ti}_2\text{O}_3$  explain why any significant mixing-induced electronic structure modifications are limited to the  $\text{VFeO}_3/\text{Me}$  and  $\text{VCrO}_3/\text{Me}$  compounds only. The strong increase of vanadium oxidation state suggests an enhanced reactivity of the supported vanadate films, which could thus be of interest in various catalytic reactions, in the same way as the oxygen-rich  $\text{V}_2\text{O}_5$  oxide is the most important industrial vanadium compound, used as a catalyst.

### 5.3 Adhesion at the HC/Me interfaces

Table 4 summarizes the adhesion energies  $E_{adh}$  (Eq. 1) of pure and mixed oxide monolayers supported on the three metal substrates as well as the misfits between the freestanding layers and metal substrate. Adhesion energies are found to be always positive (favorable to adhesion) and to span a large set of values ranging from about 1.1 eV ( $\text{Cr}_2\text{O}_3/\text{Au}$  and  $\text{CrFeO}_3/\text{Au}$ ) to more than 4.5 eV ( $\text{Ti}_2\text{O}_3/\text{Pt}$  and  $\text{TiVO}_3/\text{Pt}$ ) per formula unit. At each substrate, the adhesion of pure monolayers is systematically stronger for oxides films from the beginning of the series and, for each oxide, it tends to increase from Ag to Pt.  $E_{adh}$  of most mixed compounds are smaller than the average values of their parents ( $\delta E_{adh} < 0$  in SI, Tab. S6) – the reduction being particularly large for  $\text{TiFeO}_3/\text{Me}$  –, but in the case of  $\text{TiVO}_3/\text{Pt}$  for which mixing enhances the adhesion ( $\delta E_{adh} > 0$ ).

Since  $E_{adh}$  is calculated with respect to the corresponding freestanding oxide films at their equilibrium lattice parameters, it consists of two contributions of different nature. The first one is associated to the elastic strain of the freestanding ML necessary to match its in-plane lattice parameter with the metal substrate (Table 4) and is always unfavorable to adhesion. In the parent series, aside  $\text{Cr}_2\text{O}_3$  which displays a non-zero rumpling when freestanding and thus a reduced lateral lattice parameter, the misfit decreases from the left to the right of the series (for a given substrate) and from Pt to Ag (for a given oxide) and ranges from about

2% ( $\text{Cr}_2\text{O}_3/\text{Ag}$ ) to more than 15% ( $\text{Ti}_2\text{O}_3/\text{Pt}$ ). Misfits of the mixed monolayers show a qualitatively similar behavior and do not exceed the above ranges. However, since the lattice mismatch is accommodated mainly by the in-plane rotations and film rumpling and since the involved distortions require much less energy than bondlength compression, this contribution to  $E_{adh}$  displays small variations in each oxide series (of the order of 0.2-0.3 eV/f.u.) and, for a given oxide, its maximum variation between the three substrates is of the order of 0.2 eV/f.u. (SI, Tab. S3). Thus, it is clearly not responsible for the observed large differences of adhesion energies. The second contribution is the energy gained by bringing the strained oxide film in contact with the metal substrate. It directly represents the strength of direct metal-oxide interaction at the interface. It is favorable to adhesion in all considered cases.

While trends in adhesion may not always be easy to rationalize because they involve energy terms of different origin, Figure 8 shows a clear correlation between  $E_{adh}$  and the interfacial charge transfer  $|Q_{Me}|$ . If, in general, a weak/strong charge exchange is indeed often associated with weak/strong interfacial interaction, the present results show the existence of a unique and nearly universal  $E_{adh}(|Q_{Me}|)$  curve, which encompasses cases ranging from particularly weakly ( $\text{Cr}_2\text{O}_3$  and  $\text{Fe}_2\text{O}_3$  on Ag) to particularly strongly ( $\text{Ti}_2\text{O}_3$  and  $\text{V}_2\text{O}_3$  on Pt) interacting interfaces, regardless of the precise nature of the oxide and the metal substrate. This finding clearly demonstrates the dominant role of the direct interfacial interactions in the energetics (second contribution), driven by the cation electronegativity.

### 5.4 Energetics of mixing

Mixing energies  $E_{mix}$  (Eq. 2) have been calculated for the six metal-supported mixed oxide MLs as the energy difference between the mixed systems and the average of the two supported parents. Their values are reported in Table 5, together with the corresponding results for their freestanding counterparts from Ref. <sup>3</sup>

Depending on the oxide, we find negative or

**Table 4: Adhesion Energies  $E_{adh}$  (eV/f.u.) at the Interfaces Between the Oxide Monolayers and the Three Metal Substrates. Misfits (%) Between the Freestanding MLs and the Underlying Substrates Are Given for Reference.**

	Ti <sub>2</sub> O <sub>3</sub>	V <sub>2</sub> O <sub>3</sub>	Cr <sub>2</sub> O <sub>3</sub>	Fe <sub>2</sub> O <sub>3</sub>	TiVO <sub>3</sub>	TiCrO <sub>3</sub>	TiFeO <sub>3</sub>	VCrO <sub>3</sub>	VFeO <sub>3</sub>	CrFeO <sub>3</sub>
Ag-supported										
$E_{adh}$	2.52	1.41	1.19	1.64	1.99	1.64	1.61	1.21	1.33	1.32
misfit	10.2	7.9	2.1	7.3	7.3	9.0	8.1	6.4	7.3	6.4
Au-supported										
$E_{adh}$	3.31	1.91	1.15	1.28	2.62	2.06	1.76	1.60	1.54	1.13
misfit	10.6	8.3	2.4	7.6	7.6	9.4	8.5	6.8	7.6	6.8
Pt-supported										
$E_{adh}$	4.78	3.75	2.18	2.12	4.50	3.11	2.52	2.92	2.81	1.88
misfit	15.2	12.8	6.7	12.1	12.1	13.9	13.0	11.2	12.1	11.2

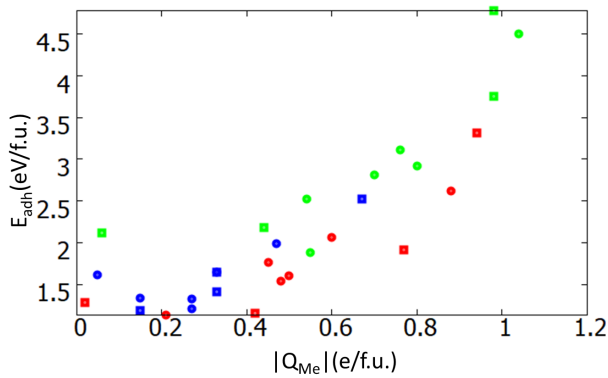


Figure 8: Adhesion energies of pure (squares) and mixed (circles) monolayers on metal substrates  $E_{adh}$  (eV/f.u.) as a function of interface charge transfer  $|Q_{Me}|$  (e/M<sub>2</sub>O<sub>3</sub> or MM'O<sub>3</sub> f.u.). Results for Ag, Au and Pt substrates are represented in blue, red and green, respectively.

830 positive mixing energies, which represent preference for cationic mixing and phase separation, respectively. If large negative  $E_{mix} \sim -$  831 0.7 eV/f.u. are found for freestanding TiFeO<sub>3</sub> 832 and VFeO<sub>3</sub> and for metal-supported VFeO<sub>3</sub>, in 833 all other cases, the mixing energies are much 834 smaller ( $|E_{mix}| < 0.4$  eV/f.u.). We find that, 835 aside few exceptions, for each mixed oxide, the 836 sign of  $E_{mix}$  is a relatively robust feature, independent of the substrate, but  $E_{mix}$  shows no 837 clear monotonic behavior along the series of ox- 838 ides or metal substrates. 839

840 We recall that in the freestanding case, the 841 large negative mixing energies found for TiFeO<sub>3</sub> 842 and VFeO<sub>3</sub> have been assigned to the existence 843

845 of a mixing-induced redox reactions which pro- 846 duce unambiguous changes of cation oxidation 847 states.<sup>3</sup> The same mechanism was also shown 848 to be at work in bulk mixed oxides<sup>25</sup> and at oxide/oxide interfaces.<sup>26</sup> For the metal-supported 849 MLs, this correlation is somewhat less clear, 850 partially due to the difficulty to unambiguously 851 identify the cation oxidation states. However, 852 the large negative  $E_{mix}$ , systematically found 853 for VFeO<sub>3</sub> on the three substrates, is consistent 854 with the enhanced oxidation of vanadium induced by the electron transfer toward the metal 855 support and/or the Fe cation, as revealed by the features of the interface electronic structure, 856 Sec. 4. Also, the strong reduction of  $|E_{mix}|$  in 857 all TiFeO<sub>3</sub>/Me systems, with respect to their 858 freestanding counterparts, correlates with the 859 suppression of the electron transfer from Ti to 860 Fe when metal-supported. Indeed, the elec- 861 tronic structure results show that the single Ti 862  $d$  electron is systematically transferred to the 863 metal substrate, so that there are no occupied 864 Ti states close to the Fermi level able to transfer 865 electrons to the iron cations. 866

867 As to broaden the perspective, Figure 9 gives 868 an overview of the calculated mixing energies in 869 the same series of bulk sesquioxides, freestanding 870 MLs, and metal-supported MLs.<sup>3,25</sup> While 871 a metal substrate enhances the preference for 872 mixing in VCrO<sub>3</sub> and reduces it for the Ti-based 873 ones, two systems clearly stand out by their 874 strongly size and support-dependent behaviors. 875 On the one hand, contrary to the bulk phase, 876 the formation of ordered mixed VFeO<sub>3</sub> MLs is 877 878

**Table 5: Mixing Energies  $E_{mix}$  (eV/f.u.) of the Six Freestanding<sup>3</sup> and Metal-Supported Mixed HC MLs.**

	TiVO <sub>3</sub>	TiCrO <sub>3</sub>	TiFeO <sub>3</sub>	VCrO <sub>3</sub>	VFeO <sub>3</sub>	CrFeO <sub>3</sub>
$E_{mix}$	+0.32	-0.16	-0.70	-0.14	-0.79	-0.16
$E_{mix}$ (Ag)	+0.12	+0.05	-0.23	-0.22	-0.60	-0.06
$E_{mix}$ (Au)	+0.13	+0.01	-0.17	-0.39	-0.74	-0.08
$E_{mix}$ (Pt)	-0.09	+0.22	+0.23	-0.27	-0.67	+0.12

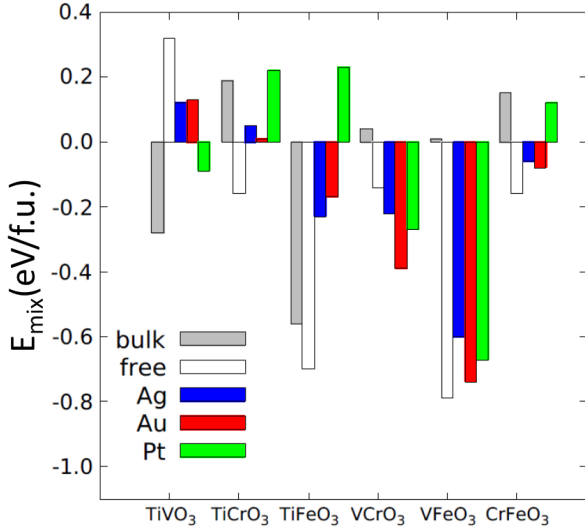


Figure 9: Mixing energies in the series of the six mixed HC oxides. Results for bulk, freestanding, Ag-, Au- and Pt-supported cases are represented in gray, white, blue, red, and green, respectively.

## 6 Conclusion

We have used a DFT+U approach to study how the presence of a metal substrate (Me = Ag, Au, Pt) modifies the structural, electronic and magnetic characteristics of a series of pure  $M_2O_3$  and mixed  $MM'O_3$  3d transition metal oxide honeycomb monolayers (M, M' = Ti, V, Cr, Fe).

We have identified general trends in the substrate-induced structural film polarization, film-support electron transfer, and oxide-metal interaction strength, and we have linked them to the behavior of the offsets between the oxide band structure (point of zero charge) and the substrate Fermi level. Accordingly, the strongest interfacial effects are found in pure and mixed oxides with the least electronegative cations (Ti and V) deposited on metal substrates with the largest work functions (Au, Pt). In these cases of Mott-Hubbard oxides, the well pronounced depletion of purely 3d Ti and V states has been rationalized by an increase of the cation oxidation state with respect to the 3+ reference.

We have also shown that the relative positions of the Fermi levels in the supported pure oxides provide a good guide for understanding the electronic redistributions in the mixed compounds. However, if the ordering of Fermi levels in the series of parent oxides is only little affected by the metal substrate, the presence of a support significantly modifies the character of oxide states in the vicinity of the Fermi level. As a consequence, aside the general trend for an electron transfer from less (Ti and V) to more (Cr and Fe) electronegative cations, valid in both freestanding and supported monolayers, the metal substrates enhance electron redistributions in V-based compounds and reduce

thermodynamically favored not only when freestanding, but also when deposited on a metallic substrate. This opens a promising route for a practical synthesis of this nano-compound. On the other hand, in the perspective of tuning the oxide mixing properties and engineering novel oxide phases, our results show that mixed compounds such as  $TiFeO_3$ , which are stable in bulk (ilmenite) and freestanding MLs, may be dramatically destabilized by the strong interaction with the metal substrate. Such a strong dependence of mixing behavior on dimensionality and substrate should impact catalytic activity originating from the so-called SMSI (Strong Metal Support Interaction) in which, under reaction conditions, metal particles are encapsulated by an ultra-thin film of the supporting oxide.

935 them in the Ti-based ones. Indeed, the fact that 977  
936  $\text{Ti}_2\text{O}_3$  gives all its valence electrons to the metal 978  
937 substrates limits any significant mixing-induced  
938 electronic rearrangements to  $\text{VCrO}_3/\text{Me}$  and 979  
939  $\text{VFeO}_3/\text{Me}$  only. Depending on the Me sub- 980  
940 strate, the modifications consist of an electron  
941 exchange between the two cations, or between 981  
942 V and the metallic support. Due to the strong  
943 modifications of their electronic structure when 982  
944 deposited on metal substrates, these vanadium  
945 mixed oxides are expected to display an en- 983  
946 hanced reactivity, of possible interest in various 984  
947 catalytic reactions. 985

948 These substrate-induced electronic effects 986  
949 have direct consequences on the energetics of 987  
950 cationic mixing. We have shown that, contrary 988  
951 to its bulk phase, the formation of ordered 989  
952 mixed  $\text{VFeO}_3$  monolayers is thermodynamically 990  
953 favored and that it is not inhibited by the pres- 991  
954 ence of a metal substrate. Conversely, metal 992  
955 support dramatically destabilizes monolayers of 993  
956  $\text{TiFeO}_3$ , a mixed oxide which is stable in bulk 994  
957 (ilmenite). Thus, not only our results show 995  
958 that metal substrates can indeed be used for  
959 engineering novel oxide phases by cationic mix- 996  
960 ing, but they also provide well-founded general 997  
961 guidelines on the link between support char- 998  
962 acteristics, the oxide electronic structure, and 999  
963 the preference for mixing or phase separation 1000  
964 in the supported oxide films. 1001

## 965 7 Acknowledgment 1002

966 We acknowledge fruitful discussions with M. R. 1003  
967 Castell, S. Wang and N. Nilius. 1004  
1005  
1006  
1007

## 968 8 Supporting Information 1008

### 969 Available 1009

970 The Supporting Information contains: 1010  
1011

- 971 • full DFT+U results for parent  $\text{M}_2\text{O}_3/\text{Me}$  1012  
972 MLs (Tabs. S1-S3) and for mixed 1013  
973  $\text{MM}'\text{O}_3/\text{Me}$  MLs (Tabs. S4-S6); 1014  
1015
- 974 • HSE03 results for parent  $\text{M}_2\text{O}_3/\text{Au}$  MLs 1016  
975 (Tab. S7, Fig. S1) and for mixed 1017  
976  $\text{MM}'\text{O}_3/\text{Au}$  MLs (Tab. S8, Fig. S2). 1018

Figs. S3-S4 are the HSE03 equivalents of  
Figs. 5 and 7 in the main text;

This material is available free of charge via the  
Internet at <http://pubs.acs.org>.

## References

- (1) Freund, H.-J.; Pacchioni, G. Oxide ultra-  
thin films on metals: new materials for  
the design of supported metal catalysts.  
*Chem. Soc. Rev.* **2009**, *37*, 2224–2242.
- (2) Netzer, F. P.; Fortunelli, A.; Eds.,  
*Oxide materials at the two-dimensional  
limit*; Springer Series in Materials Science;  
Springer International Publishing: Cham,  
Switzerland, 2016; Vol. 234.
- (3) Goniakowski, J.; Noguera, C. Intrinsic  
properties of pure and mixed monolayer  
oxides in the honeycomb structure:  $\text{M}_2\text{O}_3$   
and  $\text{MM}'\text{O}_3$  ( $\text{M}, \text{M}' = \text{Ti}, \text{V}, \text{Cr}, \text{Fe}$ ). *J.*  
*Phys. Chem. C* **2019**, *123*, 7898–7910.
- (4) Surnev, S.; Sock, M.; Kresse, G.; An-  
dersen, J. N.; Ramsey, M.; Netzer, F.  
Unusual CO adsorption sites on vana-  
dium oxide-Pd(111) “inverse model cat-  
alyst” surfaces. *The Journal of Physical  
Chemistry B* **2003**, *107*, 4777–4785.
- (5) Plessow, P. N.; Bajdich, M.; Greene, J.;  
Vojvodic, A.; Abild-Pedersen, F. Trends  
in the thermodynamic stability of ultra-  
thin supported oxide films. *The Journal of  
Physical Chemistry C* **2016**, *120*, 10351–  
10360.
- (6) Barcaro, G.; Agnoli, S.; Sedona, F.;  
Rizzi, G. A.; Fortunelli, A.; Granozzi, G.  
Structure of reduced ultrathin  $\text{TiO}_x$  polar  
films on Pt(111). *J. Phys. Chem. C* **2009**,  
*113*, 5721–5729.
- (7) Pomp, S.; Kuhness, D.; Barcaro, G.; Se-  
menta, L.; Mankad, V.; Fortunelli, A.;  
Sterrer, M.; Netzer, F. P.; Surnev, S. Two-  
dimensional iron tungstate: A ternary ox-  
ide layer with honeycomb geometry. *J.*  
*Phys. Chem. C* **2016**, *120*, 7629–7638.

- 1019 (8) Tumino, F.; Carrozzo, P.; Mascaretti, L.;<sup>1063</sup>  
1020 Casari, C. S.; Passoni, M.; Tosoni, S.;<sup>1064</sup>  
1021 Bottani, C. E.; Bassi, A. L. Two-<sup>1065</sup>  
1022 dimensional TiO<sub>x</sub> nanostructures on Au  
1023 (111): a scanning tunneling microscopy<sup>1066</sup>  
1024 and spectroscopy investigation. *2D Mate-*<sup>1067</sup>  
1025 *rials* **2015**, *2*, 045011. <sup>1068</sup>
- 1026 (9) Goniakowski, J.; Noguera, C. Properties<sup>1069</sup>  
1027 of M<sub>2</sub>O<sub>3</sub>/Au(111) honeycomb monolayers<sup>1070</sup>  
1028 (M = Sc, Ti, V, Cr, Mn, Fe, Co, Ni). *J.*<sup>1071</sup>  
1029 *Phys. Chem. C* **2019**, *123*, 9272–9281. <sup>1072</sup>
- 1030 (10) Wu, C.; Marshall, M. S. J.; Castell, M. R.<sup>1073</sup>  
1031 Surface structures of ultrathin TiO<sub>x</sub> films<sup>1074</sup>  
1032 on Au(111). *J. Phys. Chem. C* **2011**, *115*,<sup>1075</sup>  
1033 8643–8652. <sup>1076</sup>  
<sup>1077</sup>
- 1034 (11) Wang, S.; Hu, X.; Goniakowski, J.;  
1035 Noguera, C.; Castell, M. R. Influence of<sup>1078</sup>  
1036 the support on stabilizing local defects in<sup>1079</sup>  
1037 strained monolayer oxide films. *Nanoscale*<sup>1080</sup>  
1038 **2019**, *11*, 2412–2422. <sup>1081</sup>
- 1039 (12) Wang, S.; Goniakowski, J.; Noguera, C.;<sup>1082</sup>  
1040 Castell, M. R. Atomic and electronic<sup>1083</sup>  
1041 structure of an epitaxial Nb<sub>2</sub>O<sub>3</sub> honey-<sup>1084</sup>  
1042 comb monolayer on Au (111). *Physical Re-*  
1043 *view B* **2019**, *100*, 125408. <sup>1085</sup>  
<sup>1086</sup>
- 1044 (13) Köksal, O.; Baidya, S.; Pentcheva, R.<sup>1087</sup>  
1045 Confinement-driven electronic and topo-<sup>1088</sup>  
1046 logical phases in corundum-derived 3d-<sup>1089</sup>  
1047 oxide honeycomb lattices. *Phys. Rev. B*<sup>1090</sup>  
1048 **2018**, *97*, 035126. <sup>1091</sup>
- 1049 (14) Möller, C.; Fedderwitz, H.; Noguera, C.;<sup>1092</sup>  
1050 Goniakowski, J.; Nilius, N. Temperature-<sup>1093</sup>  
1051 dependent phase evolution of copper-<sup>1094</sup>  
1052 oxide thin-films on Au(111). *Phys. Chem.*<sup>1095</sup>  
1053 *Chem. Phys.* **2018**, *20*, 5636–5643. <sup>1096</sup>
- 1054 (15) Wu, C.; Castell, M. R.; Goniakowski, J.;<sup>1097</sup>  
1055 Noguera, C. Stoichiometry engineering of<sup>1098</sup>  
1056 ternary oxide ultrathin films: Ba<sub>x</sub>Ti<sub>2</sub>O<sub>3</sub><sup>1099</sup>  
1057 on Au(111). *Phys. Rev. B* **2015**, *91*,<sup>1100</sup>  
1058 155424. <sup>1101</sup>
- 1059 (16) Kresse, G.; Furthmüller, J. Efficient iter-<sup>1102</sup>  
1060 ative schemes for ab initio total energy<sup>1103</sup>  
1061 calculations using a plane-wave basis set.<sup>1104</sup>  
1062 *Phys. Rev. B* **1996**, *54*, 11169–11186. <sup>1105</sup>
- (17) Kresse, G.; Hafner, J. Ab initio molecular  
dynamics for liquid metals. *Phys. Rev. B*  
**1993**, *47*, 558–561.
- (18) Blöchl, P. E. Projector augmented-wave  
method. *Phys. Rev. B* **1994**, *50*, 17953–  
17979.
- (19) Kresse, G.; Joubert, D. From ultra-  
soft pseudopotentials to the projector  
augmented-wave method. *Phys. Rev. B*  
**1999**, *59*, 1758–1775.
- (20) Dion, M.; Rydberg, H.; Schroder, E.;  
Langreth, D. C.; Lundqvist, B. I. Van  
der Waals density functional for general  
geometries. *Phys. Rev. Lett.* **2004**, *92*,  
246401.
- (21) Klimes, J.; Bowler, D. R.; Michaelides, A.  
Chemical accuracy for the van der Waals  
density functional. *J. Phys.: Cond. Matt.*  
**2010**, *22*, 022201.
- (22) Klimes, J.; Bowler, D. R.; Michaelides, A.  
Van der Waals density functionals applied  
to solids. *Phys. Rev. B* **2011**, *83*, 195131.
- (23) Anisimov, V. I.; Aryasetiawan, F.; Liecht-  
enstein, A. I. First-principles calculations  
of the electronic structure and spectra of  
strongly correlated systems: the LDA+U  
method. *J. Phys.: Condens. Matter* **1997**,  
*9*, 767–808.
- (24) Dudarev, S. L.; Botton, G. A.;  
Savrasov, S. Y.; Humphreys, C. J.;  
Sutton, A. P. Electron-energy-loss spectra  
and the structural stability of nickel  
oxide: An LSDA+U study. *Phys. Rev. B*  
**1998**, *57*, 1505–1509.
- (25) Le, H.-L. T.; Goniakowski, J.; Noguera, C.  
Properties of mixed transition metal ox-  
ides: MM'O<sub>3</sub> in corundum-type structures  
(M, M' = Al, Ti, V, Cr, and Fe). *Phys.*  
*Rev. Mat.* **2018**, *2*, 085001.
- (26) Le, H.-L.; Goniakowski, J.; Noguera, C.  
(0001) Interfaces between M<sub>2</sub>O<sub>3</sub> corun-  
dum oxides (M = Al, Ti, V, Cr, Fe). *Surf.*  
*Sci.* **2019**, *679*, 17–23.

- 1106 (27) Heyd, J.; Scuseria, G.; Ernzerhof, M.<sup>1149</sup>  
 1107 Hybrid functionals based on a screened<sup>1150</sup>  
 1108 Coulomb potential. *J. Chem. Phys.* **2003**,  
 1109 *118*, 8207–8215. <sup>1151</sup>
- 1110 (28) Heyd, J.; Scuseria, G.; Ernzerhof, M. Er-<sup>1153</sup>  
 1111 raturum: “Hybrid functionals based on a<sup>1154</sup>  
 1112 screened Coulomb potential” [J. Chem.  
 1113 Phys. *118*, 8207 (2003)]. *J. Chem. Phys.*<sup>1155</sup>  
 1114 **2006**, *124*, 219906–219906. <sup>1156</sup>  
<sup>1157</sup>
- 1115 (29) Prada, S.; Giordano, L.; Pacchioni, G.;<sup>1158</sup>  
 1116 Noguera, C.; Goniakowski, J. Proper-<sup>1159</sup>  
 1117 ties of Pt-supported iron oxide ultra-thin<sup>1160</sup>  
 1118 films: Similarity of Hubbard-corrected<sup>1161</sup>  
 1119 and hybrid density functional theory de-<sup>1162</sup>  
 1120 scription. *J. Chem. Phys.* **2014**, *141*,<sup>1163</sup>  
 1121 144702. <sup>1164</sup>
- 1122 (30) Nilius, N.; Fedderwitz, H.; Gross, B.;<sup>1165</sup>  
 1123 Noguera, C.; Goniakowski, J. Incorrect<sup>1166</sup>  
 1124 DFT-GGA predictions of the stability<sup>1167</sup>  
 1125 of non-stoichiometric/polar dielectric sur-<sup>1168</sup>  
 1126 faces: the case of Cu<sub>2</sub>O(111). *Phys. Chem.*<sup>1169</sup>  
 1127 *Chem. Phys.* **2016**, *18*, 6729–6733. <sup>1170</sup>
- 1128 (31) Prada, S.; Giordano, L.; Pacchioni, G.;<sup>1171</sup>  
 1129 Goniakowski, J. Theoretical description of<sup>1172</sup>  
 1130 metal/oxide interfacial properties: The<sup>1173</sup>  
 1131 case of MgO/Ag(001). *Appl. Surf. Sci.*<sup>1174</sup>  
 1132 **2016**, *390*, 578–582. <sup>1175</sup>
- 1133 (32) Bader, R. F. W. A quantum theory of<sup>1176</sup>  
 1134 molecular structure and its applications.  
 1135 *Chem. Rev.* **1991**, *91*, 893–928.
- 1136 (33) Henkelman, G.; Arnaldsson, A.; Jons-  
 1137 son, H. A fast and robust algorithm for  
 1138 Bader decomposition of charge density.  
 1139 *Comput. Mater. Sci.* **2006**, *36*, 354–360.
- 1140 (34) Momma, K.; Izumi, F. VESTA 3 for three-  
 1141 dimensional visualization of crystal, vol-  
 1142 umetric and morphology data. *J. Appl.*  
 1143 *Crystallogr.* **2011**, *41*, 1272–1276.
- 1144 (35) Monkhorst, H.; Pack, J. Special points for  
 1145 Brillouin-zone integrations. *Phys. Rev. B*  
 1146 **1976**, *13*, 5188–5192.
- 1147 (36) Flores, F.; Tejedor, C. On the forma-  
 1148 tion of semiconductor interfaces. *Journal*  
*of Physics C: Solid State Physics* **1987**,  
*20*, 145–175.
- (37) Bordier, G.; Noguera, C. Electronic struc-  
 ture of a metal-insulator interface: To-  
 wards a theory of nonreactive adhesion.  
*Phys. Rev. B* **1991**, *44*, 6361–6371.
- (38) Goniakowski, J.; Noguera, C. Polariza-  
 tion and rumpling in oxide monolayers de-  
 posited on metallic substrates. *Phys. Rev.*  
*B* **2009**, *79*, 155433.
- (39) Goniakowski, J.; Noguera, C.; Gior-  
 dano, L.; Pacchioni, G. Adsorption  
 of metal adatoms on FeO(111) and  
 MgO(111) monolayers: Effects of charge  
 state of adsorbate on rumpling of sup-  
 ported oxide film. *Phys. Rev. B* **2009**, *80*,  
 125403.
- (40) Giordano, L.; Cinquini, F.; Pacchioni, G.  
 Tuning the surface metal work function by  
 deposition of ultrathin oxide films: Den-  
 sity functional calculations. *Phys. Rev. B*  
**2006**, *73*, 045414.
- (41) Giordano, L.; Pacchioni, G.; Goni-  
 akowski, J.; Nilius, N.; Rienks, E. D. L.;  
 Freund, H.-J. Interplay between struc-  
 tural, magnetic, and electronic properties  
 in a FeO/Pt(111) ultrathin film. *Phys.*  
*Rev. B* **2007**, *76*, 075416.

